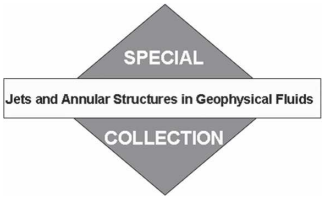

On the Arrest of Inverse Energy Cascade and the Rhines Scale

SEMION SUKORIANSKY AND NADEJDA DIKOVSKAYA

Department of Mechanical Engineering, and Perlstone Center for Aeronautical Engineering Studies, Ben-Gurion University of the Negev, Beer-Sheva, Israel

BORIS GALPERIN

College of Marine Science, University of South Florida, St. Petersburg, Florida

(Manuscript received 7 June 2006, in final form 15 December 2006)

ABSTRACT

The notion of the cascade arrest in a β-plane turbulence in the context of continuously forced flows is revised in this paper using both theoretical analysis and numerical simulations. It is demonstrated that the upscale energy propagation cannot be stopped by a β effect and can only be absorbed by friction. A fundamental dimensional parameter in flows with a β effect, the Rhines scale, L_R, has traditionally been associated with the cascade arrest or with the scale that separates turbulence and Rossby wave–dominated spectral ranges. It is shown that rather than being a measure of the inverse cascade arrest, L_R is a characteristic of different processes in different flow regimes. In unsteady flows, L_R can be identified with the moving energy front propagating toward the decreasing wavenumbers. When large-scale energy sink is present, β-plane turbulence may attain several steady-state regimes. Two of these regimes are highlighted: friction-dominated and zonostrophic. In the former, L_R does not have any particular significance, while in the latter, the Rhines scale nearly coincides with the characteristic length associated with the large-scale friction. Spectral analysis in the frequency domain demonstrates that Rossby waves coexist with turbulence on scales smaller than L_R thus indicating that the Rhines scale cannot be viewed as a crossover between turbulence and Rossby wave ranges.

1. Introduction

Terrestrial and planetary circulations are described by nonlinear equations that support various types of waves in the linear limit. The real flows exhibit a complicated interplay between turbulence and waves. While in a certain range of scales, turbulent scrambling may overwhelm the wave behavior and lead to the disappearance of the dispersion relation (such as in the small-scale range of stably stratified flows; see, e.g., Sukoriansky et al. 2005), on other scales, the wave terms cause turbulence anisotropization and emergence of systems with strong wave–turbulence interaction. Systems that combine anisotropic turbulence and waves exhibit behavior very different from that of the classical isotropic and homogeneous turbulence (McIntyre 2001). In the context of large-scale atmospheric flows, the interaction between turbulence and waves yields dynamically rich macroturbulence (Held 1999; Schneider 2006), the notion that underlies diverse phenomena ranging from a local weather to a global climate. The subtlety of this interaction is further highlighted by the fact that, because of the planetary rotation and Taylor–Proudman theorem, large-scale flows are quasi-two-dimensionalized and may be conducive to the development of the inverse energy cascade (Read 2005). One of the parameters that characterize macroturbulence is the Rhines wavenumber, $k_R = (\beta/2U)^{1/2}$, or the Rhines scale, $L_R \sim k_R^{-1}$, where U is the rms fluid velocity, and β is the northward gradient of the Coriolis parameter (Rhines 1975; in the original paper, this wavenumber was denoted by k_β; here, k_R is used instead, as the notation k_β is reserved for another wavenumber to appear later). At this scale, the inverse cascade supposedly becomes arrested, and the nonlinear turbulent behavior is replaced by excitation of lin-

Corresponding author address: Semion Sukoriansky, Department of Mechanical Engineering, Ben-Gurion University of the Negev, Beer-Sheva 84105, Israel.
E-mail: semion@bgu.ac.il

DOI: 10.1175/JAS4013.1

ear Rossby waves. This scale has also been associated with flow reorganization into the bands of alternating zonal jets, the process known as zonation, and the width of the jets has often been scaled with k_R^{-1}. The Rhines scale plays a prominent role in many theories of large-scale atmospheric and oceanic circulation (see, e.g., James and Gray 1986; Vallis and Maltrud 1993; Held and Larichev 1996; Held 1999; Lapeyre and Held 2003; Schneider 2004; LaCasce and Pedlosky 2004; Vallis 2006) as well as in theories of planetary circulations (see, e.g., the review by Vasavada and Showman 2005) and, possibly, even stellar convection (see, e.g., Miesch 2003).

The meaning of the Rhines scale is not always clear, however. Even in the barotropic case, different regimes would arise for continuously forced and decaying flows, for flows with and without friction, and for flows in bounded and unbounded domains. As a result, the Rhines scale may be time-dependent, stationary, or entirely obscured by friction. In many studies, the scaling with k_R^{-1} is implied but the coefficient of proportionality varies in a wide range. There also exists a multitude of other scaling parameters that characterize various aspects of the flow and flow regimes. It is important, therefore, to understand the hierarchy of these parameters and the place of k_R in this hierarchy. This is precisely the goal of the present study. This goal cannot be achieved without clarification of the notion of the arrest of the inverse energy cascade by the Rossby wave propagation, which, thus, becomes another focal point of this study. Both issues will be addressed theoretically; the theoretical results will be substantiated in numerical simulations.

The paper is organized in the following fashion. The next section presents the basics of the theory of two-dimensional (2D) turbulence with a β effect and accentuates its problems. Section 3 presents analysis of the interaction between inverse energy cascade of 2D turbulence and Rossby waves and discusses the notion of the cascade arrest. Section 4 elaborates this analysis and clarifies the meaning of the Rhines scale using numerical simulations of barotropic 2D turbulence on the surface of a rotating sphere. In addition, that section describes the hierarchy of scaling parameters and corresponding flow regimes as well as the interaction between turbulence and Rossby waves in different regimes. Finally, section 5 presents discussion and some conclusions.

2. Turbulence and Rossby waves: The basics

The interaction between 2D turbulence and Rossby waves has been considered in the pioneering study by Rhines (1975). Starting with the barotropic vorticity equation on a β plane, he concentrated on mainly unforced barotropic flows caused by initially closely packed fields of eddies spreading from a state with a δ function–like spectrum peaked at some wavenumber k_0. Among the major conclusions of the paper, the following have the most relevance to the present study:

1) At the wavenumber, denoted as k_R, at which the root-mean-square velocity U is equal to the phase speed of Rossby waves with an average orientation, $c_p = \beta/2k^2$, there exists a subdivision of the spectrum on turbulence ($k > k_R$) and wave ($k < k_R$) modes.
2) The expansion of the flow field to k_R triggers wave propagation and slowing down, or the arrest, of the cascade to smaller wavenumbers.
3) Triad interactions of the modes with wavenumbers close to k_R require simultaneous resonance in wavenumbers and frequencies.
4) On average, triad interactions transfer energy to modes with smaller frequencies and smaller wavenumbers causing the anisotropization of the flow field. As a result, the energy accumulates in modes with small north–south wavenumbers that correspond to east–west currents, zonal jets, giving rise to the process of zonation.
5) The width of the zonal jets scales with k_R^{-1}.
6) In a steadily forced flow, the spectrum is expected to develop a sharp peak at k_R and rapidly decrease for $k > k_R$.

Items 3 and 4 have been confirmed in numerous theoretical, numerical, and experimental studies (see, e.g., Williams 1975, 1978; Holloway and Hendershott 1977; Panetta 1993; Vallis and Maltrud 1993; Chekhlov et al. 1996; Cho and Polvani 1996; Nozawa and Yoden 1997; Huang and Robinson 1998; Huang et al. 2001; Read et al. 2004; Vasavada and Showman 2005; Galperin et al. 2006). A new light on zonation was shed by Balk (2005). Exploring a new invariant for inviscid 2D flows with Rossby waves (Balk 1991; Balk and van Heerden 2006), he showed that the transfer of energy from small to large scales takes place in such a way that most of the energy is directed to the zonal jets. The rest of the aforementioned issues, however, remain controversial, particularly when compounded with other complicating factors such as the friction, continuous forcing, effects of the boundaries, effects of stratification, etc. Let us consider, for example, a realistic system in which the bottom friction acts like a large-scale drag. One can introduce a wavenumber associated with that drag, $k_{\rm fr}$, as a wavenumber at which the characteristic friction time is equal to that of the flow. If $k_{\rm fr} > k_R$ then the frictional processes would forestall the arrest and the

Rhines scale would require modification (James and Gray 1986; Danilov and Gurarie 2002; Smith et al. 2002). In flows with continuous small-scale forcing at a rate ϵ, the equilibrium between the eddy turnover time and the Rossby wave period selects an anisotropic transition wavenumber with an amplitude $k_\beta \propto (\beta^3/\epsilon)^{1/5}$ (the proportionality coefficient will be established later); its angular distribution resembles a dumbbell (Vallis and Maltrud 1993; Holloway 1986; Vallis 2006). The introduction of k_β raises a slew of new questions. If there is an arrest in the forced flows, which one of the two wavenumbers, k_R and k_β, should be associated with the arrest scale? At which scale is the anticipated in item 2 Rossby wave excitation triggered? Can Rossby waves coexist with turbulence on scales intermediate between k_R^{-1} and k_β^{-1}? With regard to item 5, one may ask which one of these two wavenumbers should be used as a scaling parameter for the width of the zonal jets? Indeed, although the mechanism of zonation has by now been solidly established, the scaling of the jets' width with the Rhines scale has not been conclusive as the coefficient of proportionality has so far been elusive. For instance, Hide (1966) used a scale similar to k_R^{-1} for the width of the equatorial jets on Jupiter and Saturn while Williams (1978) and others applied it to the off-equatorial jets. Conclusive scaling with k_R^{-1} has materialized neither in the Grenoble experiment (Read et al. 2004) nor in the recent analysis of the eddy-resolving simulations of oceanic jets by Richards et al. (2006).

Chekhlov et al. (1996) have scrutinized the notion of the arrest of the inverse energy cascade and asserted that Rossby wave excitation cannot halt the cascade in principle. On the other hand, they have confirmed that the β term in the vorticity equation impedes triad interactions hence reducing the effectiveness of nonlinear transfers and increasing their characteristic time scale. Furthermore, Chekhlov et al. (1996), Smith and Waleffe (1999), and Huang et al. (2001) have shown that the spectrum of forced β-plane turbulence is strongly anisotropic. On large scales, the spectrum of the zonal modes is proportional to $\beta^2 k_y^{-5}$. It is important to understand the synergy between the slowing-up of the nonlinear interactions and spectrum steepening. The reduction in the effectiveness of the triad interactions is due to the requirement of the simultaneous resonance in wavenumbers and frequencies (Rhines 1975, 1979; Holloway and Hendershott 1977; Carnevale and Martin 1982). The ensuing cascade anisotropization facilitates strong energy flux to the zonal modes (Rhines 1975; Vallis and Maltrud 1993; Chekhlov et al. 1996). Because of the frequency resonance impediment, however, the zonal modes cannot effectively transfer their energy to other modes. Since the total energy flux must be conserved, the spectral energy density of the zonal modes has to increase. The steepening of the zonal spectrum eventually reaches the $\beta^2 k_y^{-5}$ distribution at which the frequency resonance condition is relaxed and the zonal modes can again efficiently exchange energy with other modes. This exchange allows for the zonal modes to dispose of the energy exceeding the $\beta^2 k_y^{-5}$ levels and maintain a steady and statistically stable flow regime (Huang et al. 2001). The $\beta^2 k_y^{-5}$ spectrum is somewhat reminiscent of the isotropic -5 distribution discussed by Rhines (1975). He has put the existence of such a sharp slope in doubt, however, because it would imply a strong dependence on the smallest wavenumbers with the highest energy levels, which would lead to a strong nonlocality negating the dimensional arguments that facilitated the isotropic $\beta^2 k^{-5}$ dependence in the first place. Sukoriansky et al. (2002) have elucidated that in the case of an anisotropic spectrum, the arguments of nonlocality may not be applicable hence one could expect that a flow regime with a steep zonal spectrum,

$$E_Z(k_y) = C_Z \beta^2 k_y^{-5}, \tag{1}$$

may be established [here, C_Z is an $O(1)$ coefficient]. The stability of such a regime is stipulated by the Rayleigh–Kuo criterion (Chekhlov et al. 1996; Huang et al. 2001; McWilliams 2006). Furthermore, similarly to Lilly (1972) in the case of isotropic, nonrotating flows, Sukoriansky et al. (2002) have argued that only the large-scale drag can balance the inverse cascade and facilitate the establishment of a steady state in flows with a β effect. They have reproduced the spectrum (1) in forced, dissipative simulations of 2D barotropic turbulence with a linear drag on the surface of a rotating sphere and showed that in such flows, k_R is close to k_{fr}. They have also found an evidence of the spectrum (1) on all four solar giant planets. Later, using the eddy-resolving simulations by Nakano and Hasumi (2005) of the North Pacific Ocean, Galperin et al. (2004) have shown that this spectrum may also be present in the barotropic mode of the subsurface oceanic alternating zonal jets.

Considering a space of parameters that characterize different regimes in barotropic, forced and dissipative β-plane turbulence, Galperin et al. (2006) have found that in a certain subspace, a flow attains a universal regime with the zonal spectrum (1) and $C_Z \simeq 0.5$. This subspace is wide enough to include important laboratory, terrestrial, and planetary flows (Galperin et al. 2006).

Despite the progress made in understanding of vari-

ous aspects of β-plane turbulence, there still remains a great deal of confusion regarding the arrest of the inverse energy cascade and the Rhines scale. The fact that the interplay between turbulence and Rossby waves has never been thoroughly investigated only adds to this confusion. The next section gathers some theoretical arguments that may help to clarify this perplexity. In section 4, these arguments will be substantiated via numerical experimentation.

3. Is the cascade really arrested?

The cascade arrest is often understood as a transition of a flow character from strongly nonlinear and turbulent to weakly nonlinear and wave-dominated under the action of a nondissipative extra strain in the Bradshaw (1973) terminology, a β effect. This transition presumably takes place at a scale k_R^{-1}. Such an interpretation applies to unforced flows considered by Rhines (1979) in great detail (see also Majda and Wang 2006, chapters 10–13). Rhines (1979) showed that in unforced flows, both the nonlinear term and a rate of the energy transfer to large scales decrease with time. This tendency can be traced to the impediment to triad interactions caused by the frequency resonance condition discussed in the previous section. A soft transition from a strongly nonlinear to a weakly nonlinear regime takes place at the crossover wavenumber, k_R (Rhines 1979). This interpretation of the cascade arrest is sometimes applied to forced flows (James and Gray 1986). The extension of the results valid for the unforced dynamics ($\epsilon = 0$) to flows with continuous forcing ($\epsilon \neq 0$) may be problematic however. Already at the level of the dimensional analysis, the presence of the nonzero ϵ and appearance of the nontrivial wavenumber k_β point to significant differences between the two cases. Vallis and Maltrud (1993) have first recognized the importance of the transitional wavenumber, k_β. In their forced dissipative simulations, Vallis and Maltrud (1993) observed a "piling up" of the computed energy spectrum in the vicinity of k_β. This piling up took place in a short range of wavenumbers, however, because the simulation parameters were set such that k_β was close to k_R. The spectral steepening was thought to be a result of the dumbbell becoming a barrier to the energy flux to larger scales. Chekhlov et al. (1996) investigated a regime with $k_\beta \gg k_R$. They have also observed the energy piling up in the vicinity of k_β but they have attributed this phenomenon to a development of a new regime of circulation with the steep spectrum (1). Chekhlov et al. (1996) have emphasized that although the total upscale energy flux in forced, undamped flows remains constant, the rate of the energy front propagation decreases due to the steepening of the zonal spectrum. The inverse cascade anisotropization combined with the zonal spectrum's steepening facilitates the establishment of the zonostrophic regime in flows with a large-scale drag (Galperin et al. 2006).

Although the frequency resonance constraint impedes the triad interactions in both forced and unforced flows, it does not cause the arrest of the inverse energy cascade, which continues to pump energy to ever-larger scales at a constant rate ϵ. The frequency resonance impediment only facilitates the funneling of the energy flux into the zonal modes leading to spectral anisotropization (Chekhlov et al. 1996) and reorganization of the flow field into a lower-dimensional slow manifold decoupled from the fast Rossby waves (Smith and Lee 2005). This manifold manifests itself as a system of quasi-one-dimensional alternating zonal jets. The threshold of the spectral anisotropization is characterized by the wavenumber k_β while the width of the zonal jets is determined by the large-scale friction (Sukoriansky et al. 2002). It is important to emphasize that forced β-plane turbulence never collapses to a linear state since the nonlinearity is the very factor that sustains the slow manifold. It is clear, therefore, that a β effect cannot halt the inverse energy cascade (Chekhlov et al. 1996; Sukoriansky et al. 2002; Galperin et al. 2006).

In the remainder of this section, we shall elaborate various scaling relationships pertinent to forced anisotropic turbulence with a β effect. These relationships will be used to further elucidate the absence of the cascade arrest. The flows will be assumed to contain a stationary random forcing maintaining an inverse energy cascade at a constant rate ϵ. This case has most relevance to the real world large-scale terrestrial and planetary circulations (Galperin et al. 2006). The importance of the parameter ϵ is underscored by the conjecture that the diffusion coefficient of the poleward heat transport strongly depends on it (Held and Larichev 1996; Held 1999; Lapeyre and Held 2003).

Two classes of flows will be considered, those without and with the action of the large-scale drag. The first class is rather unrealistic because, first, some kind of a drag is always present in all real flows, and, second, the large-scale energy condensation would eventually distort flow configuration in long-term integrations (Smith and Yakhot 1993, 1994). Such flows are important, however, for understanding of the dynamics of the transients and mechanisms that lead to the establishment of observable long-term patterns. These patterns are represented in the second class of flows.

Barotropic, small-scale forced, anisotropic 2D turbulence on a β plane where x and y are directed eastward

and northward, respectively, is described by the vorticity equation,

$$\frac{\partial \zeta}{\partial t} + \frac{\partial(\nabla^{-2}\zeta, \zeta)}{\partial(x, y)} + \beta \frac{\partial}{\partial x}(\nabla^{-2}\zeta) = D + \xi, \qquad (2)$$

where ζ is the vorticity, ξ is the forcing, and D is the friction that includes a small-scale and a large-scale components. In numerical simulations, the small-scale part of D is usually represented by a hyperviscous term while the large-scale drag is linear. As was shown by Sukoriansky et al. (1999, 2002), a linear drag, being a physically plausible mechanism of the large-scale energy damping due to the bottom friction, is a soft process that introduces only a small distortion to the inverse energy cascade that does not lead to a spurious accumulation of energy in the lowest resolved modes. The constant β in (2) is the northward gradient of the Coriolis parameter, f, $f = f_0 + \beta y$, where f_0 is a reference value of f. The forcing ξ, concentrated around some high wavenumber k_ξ and assumed to be random, zero-mean, Gaussian and white noise in time, supplies energy to the system at a constant rate. Part of this energy sustains the inverse cascade with the rate ϵ while the other part is lost on scales $k > k_\xi$ due to the small-scale dissipation.

On its left-hand side, Eq. (2) contains the nonlinear and the β terms that are dominant in different ranges of scales. Here, the balance between these terms will be analyzed using the notion of the characteristic time scale rather than the characteristic velocity as in Rhines (1975). The relatively high wavenumber modes are nearly isotropic and obey the classical Kolmogorov–Batchelor–Kraichnan (KBK) theory of 2D turbulence in the energy range. For those modes, a conventionally defined eddy turnover time, $\tau_t(k)$, is a ratio of the local length scale, k^{-1}, and the local velocity scale, $U(k)$, which can be estimated from the KBK energy spectrum $E(k)$, $U(k) \propto [k\mathrm{E}(k)]^{1/2}$, yielding $\tau_t(k) = [k^3\mathrm{E}(k)]^{-1/2}$, where

$$E(k) = C_K \epsilon^{2/3} k^{-5/3}. \qquad (3)$$

Here, $C_K \simeq 6$ is the Kolmogorov–Kraichnan constant. Equating τ_t and the Rossby wave period, $\tau_{\mathrm{RW}}(\mathbf{k}) \propto -k^2/\beta k_x$, one can find a crossover wavenumber for the β effect induced anisotropy (Vallis and Maltrud 1993),

$$k_\beta \propto (\beta^3/\epsilon)^{1/5}. \qquad (4)$$

Note that for a stationary ϵ, k_β is also stationary even if the flow itself is not in a steady state. Other characteristic wavenumbers for both unsteady and steady-state flows are k_ξ and k_d, where the latter is associated with the small-scale dissipation. For steady-state flows, this group should also include the large-scale friction wavenumber, k_{fr}.

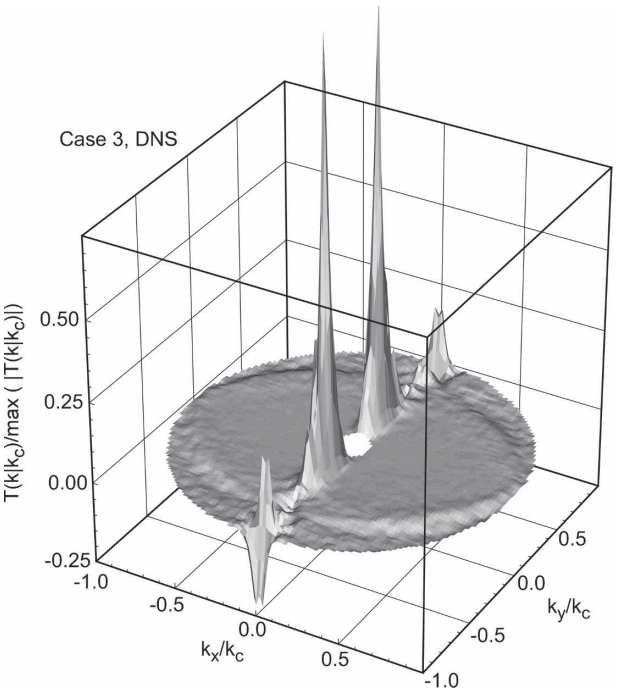

FIG. 1. Normalized spectral energy transfer, $\mathcal{T}_E(\mathbf{k}|k_c)/\max|\mathcal{T}_E(\mathbf{k}|k_c)|$, for $k_c = 50$.

Simulations by Chekhlov et al. (1996), Smith and Waleffe (1999), and Huang et al. (2001) of the evolving turbulence with a β effect have shown that as the energy propagates to wavenumbers smaller than k_β, the nature of the flow and its spectral characteristics change markedly. At a wavenumber close to k_β, the zonal spectrum, $E_Z(k_y)$, undergoes reorganization and attains a steep distribution (1) while the nonzonal, or the residual spectrum largely preserves the shape given by the KBK law, Eq. (3).

The anisotropization of the inverse cascade has been demonstrated using the results of direct numerical simulation (DNS) of a β-plane turbulence by Chekhlov et al. (1996) who considered the energy transfer function, $\mathcal{T}_E(\mathbf{k}|k_c)$. This function describes the $\mathbf{k}$-dependent spectral energy flow from all modes with $k > k_c$ to a given mode $\mathbf{k}$, $k < k_c$. The value of k_c is set arbitrarily but such that $k_c < k_\xi$. Figure 1 shows $\mathcal{T}_E(\mathbf{k}|k_c)$ for a simulation with $k_c = 50$ (which was smaller than $k_\beta = 79$). The hole in the middle of the Fig. 1 indicates that the energy front had not yet reached those wavenumbers. There is a striking difference between energy transfer to zonal modes $k_x \to 0$ and the rest of the modes. One can see that most of the energy flux is directed toward the zonal modes; the trend that dramatically increases with decreasing k.

The spectral energy transfer has also been calculated by Read et al. (2007) using the data from the Grenoble experiment (Jets special collection). In qualitative similarity to Fig. 1, they obtained an anisotropic distribution of $\mathcal{T}_E(\mathbf{k}|k_c)$ peaking at small k_y.

As a result of the spectral anisotropization, the zonal energy on the large scales exceeds its nonzonal counterpart, and the total energy, $E_{\text{tot}}(t)$, can be estimated based upon the zonal energy spectrum only,

$$E_{\text{tot}}(t) \simeq \frac{U^2(t)}{2} \simeq \sum_{k_m}^{k_d} E_Z(k_y) \propto \beta^2 k_m^{-4}(t), \tag{5}$$

where $U(t)$ is the rms of the zonal velocity, and $k_m(t)$ is the smallest wavenumber with the spectrum (1) at time t. As follows from (5),

$$k_m(t) \propto [\beta/2U(t)]^{1/2} = k_R(t), \tag{6}$$

and so one concludes that in unsteady flows with the zonal spectrum (1), the Rhines wavenumber, k_R, is time-dependent and provides the location of the moving energy front. Clearly, Eq. (6) does not imply the arrest of the inverse cascade; in an unbounded domain, after sufficiently long time, k_R can attain an arbitrarily small value. The unsteady flow under consideration highlights the difference between k_R and k_β; not only is k_R time dependent while k_β is stationary, but k_R may become much smaller than k_β.

Combining (5) with the linear trend $E_{\text{tot}}(t) = \epsilon t$, one obtains

$$k_m(t) \propto k_R(t) \propto \beta^{1/2}(\epsilon t)^{-1/4}. \tag{7}$$

A similar estimate of the evolution of the moving energy front for the classical KBK turbulence with no rotation yields the $-3/2$ law (Rose and Sulem 1978),

$$k_m^0(t) \propto \epsilon^{-1/2} t^{-3/2}. \tag{8}$$

Comparing the $-1/4$ and $-3/2$ evolution laws, Eqs. (7) and (8), respectively, one concludes that rather than halting the inverse cascade, a β effect only slows down the upscale march of the energy front. The deceleration of the energy front propagation is caused by the prolongation of the time stretch necessary to saturate the zonal modes to their energy levels specified by the spectrum (1) [instead of (3)] at the same rate of the energy transfer, ϵ. As a consequence, numerical simulations on a β plane or on the surface of a rotating sphere require much longer integration time than similar simulations with no rotation; this tendency is reflected in the $-1/4$ law (7).

When a large-scale drag is present, an ensuing steady-state flow regime is determined by the ratios between k_{fr}, k_β, k_d, and k_ξ (Galperin et al. 2006). There exists a certain subspace of these parameters in which a flow undergoes zonation and develops a universal stationary regime whose anisotropic spectrum in the β-dominated range $k_{\text{fr}} < k < k_\beta$ approaches a distribution given by Eqs. (1) and (3). The steep zonal spectrum is better pronounced for $k_{\text{fr}} \ll k_\beta$; it also extends to the region $k > k_\beta$ to its intersection with the KBK, isotropic, modal $k^{-8/3}$ spectrum as explained in Sukoriansky et al. (2002). The parameter subspace of this regime is delineated by three conditions: 1) the β-dominated range is sufficiently wide; 2) the forcing operates on scales not impacted upon by the β effect; and 3) the frictional wavenumber is large enough [$k_{\text{fr}} \gtrsim 4(2\pi/L)$, L being the system size] to avoid the large-scale energy condensation (Smith and Yakhot 1993, 1994). For convenience, Galperin et al. (2006) have coined this regime *zonostrophic*. Sukoriansky et al. (2002) have shown that for this regime, the friction wavenumber, k_{fr}, is the final destination of the moving energy front given by Eq. (7), and thus $k_R \sim k_{\text{fr}}$. The latter relationship will be confirmed in the next section. Similarly to the unsteady regime, k_R is not a scale of inverse cascade termination by a β effect; the advance of the energy front can only be stopped by the large-scale drag. Outside the zonostrophic regime, the flow depends on some additional parameters and k_R ceases to be the final destination of the moving energy front; the latter is still associated with k_{fr}, however.

From the previous studies and the scaling arguments in this section, we draw two main conclusions: 1) in unsteady flows, the marching in time of the moving energy front slows down from the $-3/2$ to $-1/4$ law upon crossing of k_β and the front's location can be related to k_R; 2) in steady flows, k_R can be identified with k_{fr} in the zonostrophic regime. These conclusions will be confirmed in numerical simulations of barotropic 2D turbulence on the surface of a rotating sphere described in the next section. In addition, using the frequency analysis in Fourier space, an analysis of the interplay between turbulence and Rossby waves will also be presented.

4. Turbulence and Rossby waves: Results of numerical simulations

This section describes numerical experimentation with two-dimensional turbulent flows on the surface of a rotating sphere. The flow is governed by the barotropic vorticity equation,

$$\frac{\partial \zeta}{\partial t} = -J(\psi, \zeta + f) + \nu\nabla^{2p}\zeta - \lambda\zeta + \xi, \tag{9}$$

where ζ is the vorticity, ψ is the streamfunction defined as $\nabla^2\psi = \zeta$; $f = 2\Omega\sin\theta$ is the Coriolis parameter (or the planetary vorticity), Ω is the angular velocity of the sphere's rotation; ν is the hyperviscosity coefficient, p is the power of the hyperviscous operator (p was either 4 or 8 in this study), λ is the linear friction coefficient, and ξ is the small-scale forcing, respectively. In addition, $J(\psi, \zeta + f)$ is the Jacobian representing the nonlinear term, $J(A, B) = (R^2\cos\theta)^{-1}(A_\phi B_\theta - A_\theta B_\phi)$, and R is the sphere's radius. For convenience, the unit of length is set to be the radius of the sphere. In these units, $R = 1$ and will be omitted in the forthcoming derivations. The natural time scale is $T = \Omega^{-1}$ such that $\Omega = 1$. To explore the explicit dependency on Ω, in some of the experiments T was kept fixed while Ω varied.

On the surface of a unit sphere, the streamfunction can be represented via the spherical harmonics decomposition,

$$\Psi(\mu, \phi, t) = \sum_{n=1}^{N} \sum_{m=-n}^{n} \psi_n^m(t) Y_n^m(\mu, \phi), \qquad (10)$$

where $Y_n^m(\mu, \phi)$ are the spherical harmonics (the associated Legendre polynomials), $\mu = \sin\theta$, ϕ is the longitude, θ is the latitude, n and m are the total and zonal wavenumbers, respectively, and N is the total truncation wavenumber. Conventionally, the indices n, m, and N are nondimensional. However, when appear in equations below, the wavenumbers n and m have the dimension of the inverse length. Since in our units $R = 1$, we shall not differentiate between the indices and wavenumbers.

In the unforced, nondissipative, linear limit, Eq. (9) gives rise to Rossby waves whose dispersion relation is

$$\omega_{m,n} = -2\beta \frac{m}{n(n+1)}, \qquad (11)$$

where $\beta = \Omega/R$. We shall retain β in the forthcoming equations in order to preserve the transparency between the cases of a β plane and rotating sphere.

The wavenumber $n_\beta \propto (\beta^3/\epsilon)^{1/5}$ is the analog of k_β. In the forced, dissipative regime, the balance between the small-scale forcing and large-scale dissipation gives rise to a steady state. The kinetic energy spectrum can be calculated as

$$E(n) = \frac{n(n+1)}{4} \sum_{m=-n}^{n} \langle |\psi_n^m|^2 \rangle, \qquad (12)$$

where the brackets indicate an ensemble or time average (Boer 1983; Boer and Shepherd 1983). This spectrum can be represented as a sum of the zonal and residual spectra, $E(n) = E_z(n) + E_R(n)$, where the zonal spectrum, $E_z(n)$, corresponds to the addend with $m = 0$. In unsteady flows (Huang et al. 2001) and in the inertial range of the zonostrophic regime (Sukoriansky et al. 2002; Galperin et al. 2006) these spectra are similar to those in β-plane turbulence,

$$E_Z(n) = C_Z \beta^2 n^{-5}, \quad C_Z \sim 0.5, \qquad (13a)$$

$$E_R(n) = C_K \epsilon^{2/3} n^{-5/3}, \quad C_K \sim 5 \text{ to } 6. \qquad (13b)$$

The zonal and residual spectra intersect at the transitional wavenumber,

$$n_\beta = \left(\frac{C_Z}{C_K}\right)^{3/10} \left(\frac{\beta^3}{\epsilon}\right)^{1/5} \simeq 0.5 \left(\frac{\beta^3}{\epsilon}\right)^{1/5}. \qquad (14)$$

To investigate the energy front propagation in unsteady flows, a series of long-term simulations was performed using Eq. (9) decomposed in spherical harmonics according to Eq. (10). A Gaussian grid was employed with resolutions of 400×200 and 720×360 nodes and 2/3 dealiasing rule (rhomboidal truncations R133 and R240, respectively). The hyperviscosity coefficient, ν, was chosen such as to effectively suppress the enstrophy range. The Gaussian random forcing was distributed amongst all modes $n_\xi = 83, 84, 85$ and $n_\xi = 99, 100, 101$ for R133 and R240, respectively; it had a constant variance and was uncorrelated in time and between the modes.

TABLE 1. Parameters of the four runs shown in Fig. 4.

Experiment	Ω	ϵ	n_β
1	1	1.44×10^{-8}	17.6
2	1	2.58×10^{-9}	24.8
3	2.5	1.42×10^{-8}	30.6
4	3	1.44×10^{-8}	34.1

The values of the parameters used in unsteady simulations are summarized in Table 1. In total, four numerical experiments were performed. Although Ω and ϵ varied in a wide range in these experiments, their values were set such as to ensure $n_\beta < n_\xi$. For statistical analysis of the results, ensemble averaging over 80 to 110 independent realizations was employed.

At first, the energy evolution was investigated. It is well known that without rotation, the total energy of the flow increases linearly with time, $E_{\text{tot}}(t) = \epsilon t$. We wanted to verify that, first, the linear trend is preserved in the case of nonzero rotation and, second, the zonal and nonzonal total energy components, $E_{\text{tot}}^Z(t)$ and $E_{\text{tot}}^R(t)$ respectively, would follow a similar trend [here, $E_{\text{tot}}(t) = E_{\text{tot}}^Z(t) + E_{\text{tot}}^R(t)$; $E_{\text{tot}}^R(t)$ contains both the eddy and wave energies]. Figure 2 shows the evolution of the total energy and its components for experiment 1 in a simulation of the duration of 10 000 planetary days

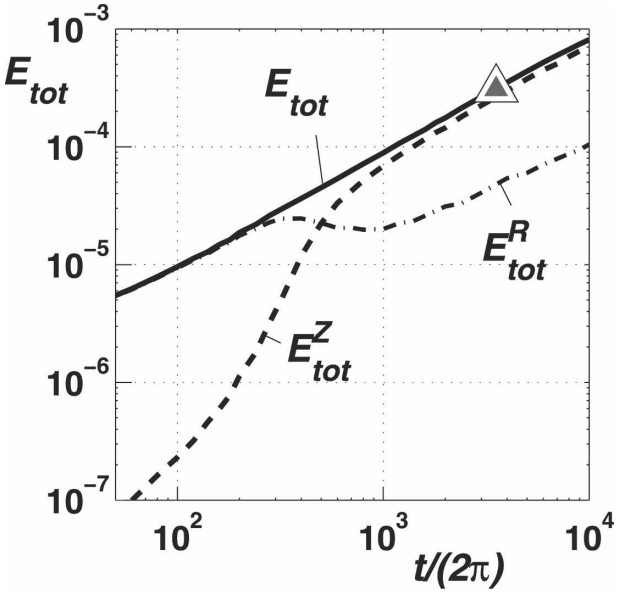

FIG. 2. Evolution of the total energy, $E_{tot}(t)$ (thick solid line), and its zonal (dashed line) and nonzonal (dashed–dotted line) components, $E^Z_{tot}(t)$ and $E^R_{tot}(t)$, respectively, in experiment 1. A triangle on $E_{tot}(t)$ shows the time required for the energy front to reach the largest scales in the system in the case when $\beta = 0$ but ϵ is the same as in experiment 1.

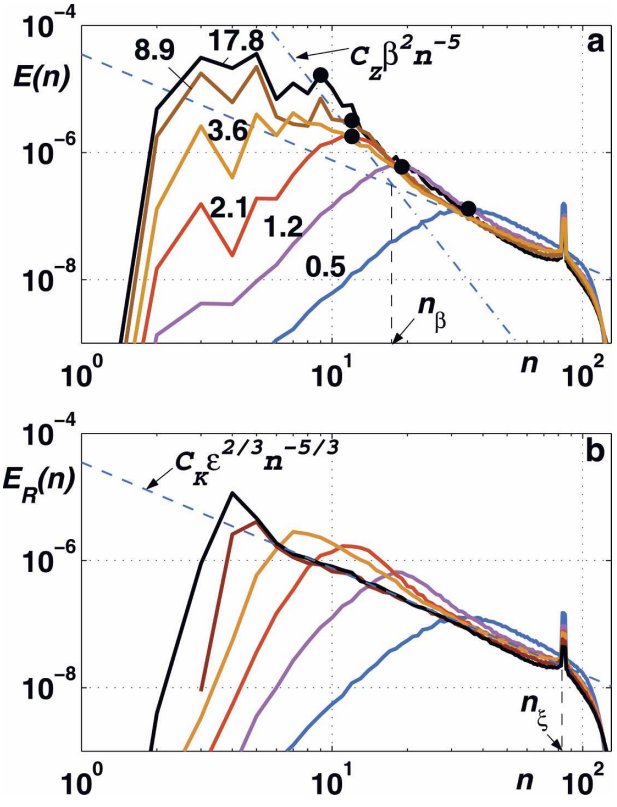

FIG. 3. (a) Total and (b) nonzonal energy spectra at different times in experiment 1 of unsteady simulations ($\lambda = 0$). The spectra are marked by the total energy ($\times 10^5$) accumulated in the flow field from the beginning of simulations. Black dots show the location of the energy front n_m. The transition from the $-5/3$ to -5 slope around n_β is clearly visible in (a). Before the transition, the spectral energy density rapidly decreases for $n < n_m$. After the transition, the energy accumulates at the modes $n < n_m$ facilitating the emergence of the plateau.

(for experiment 1, 1 day $= 2\pi$T). Initially, the zonal energy is very small and the entire energy is mostly concentrated in the nonzonal component. That component at first grows linearly, then temporarily preserves an approximately constant value and then returns to a linear growth while remaining considerably smaller than $E_{tot}(t)$. At those later times, the total energy is mostly contained in the zonal component. Generally, after initial restructuring, both $E^Z_{tot}(t)$ and $E^R_{tot}(t)$ grow linearly in time for as long as the flow evolution remains unobstructed by the action of a large-scale drag or domain boundaries.

We have conducted an additional simulation featuring $\beta = 0$ and the same ϵ as the one used in experiment 1. The evolution of the total energy in that simulation was indistinguishable from the case with $\beta \neq 0$. The only difference was that in the case $\beta = 0$, the energy front required much shorter time to reach the largest scales of the system. The total energy at that moment is marked by a triangle in Fig. 2. Clearly, the shortening of the evolution time is a result of the fast front propagation described by Eq. (8). For $\beta \neq 0$, the system can accumulate significantly higher energy; according to Eq. (5), this energy scales with β^2 and is independent of ϵ. This increased energetic capacity of the system is a direct result of the spectral anisotropization and steepening of the zonal spectrum according to Eq. (1).

The behavior of the total energy components exhibited in Fig. 2 requires some clarification. Further insight comes from the consideration of the evolution of the total and residual energy spectra for the same experiment 1 shown in Fig. 3. Driven by the inverse cascade, the spectrum expands toward the small wavenumber end. Until the transitional wavenumber n_β is reached, the energy front, $n_m(t)$, marked by the black dots in Fig. 3a, can be identified as a wavenumber with the highest energy. For $n < n_m$, the spectral energy density rapidly decreases. As in classical 2D turbulence, the ensemble-averaged spectra at the wavenumbers swept by n_m remain in a quasi–steady state. The approximate observance of the classical isotropic KBK distribution (13b) is an indication that a β effect does not yet have a strong influence on these scales. This behavior changes when n_m becomes smaller than n_β. The spectrum begins to steepen eventually attaining the level dictated by

Eq. (13a). As discussed earlier, the saturation of the spectrum at this level is a slow process during which the energy transfer continues not only to the mode n_m but also to the modes with $n < n_m$. As a result, along with the slope (13a), the energy spectrum also forms a plateau for $n \lesssim n_m$. Let us emphasize that the moving energy front n_m is not only a transitional wavenumber between the -5 slope and a plateau but it also corresponds to the number of the zonal jets (Chekhlov et al. 1996).

By comparing Figs. 2 and 3, we establish that the aforementioned change in the behaviors of $E^Z_{\rm tot}(t)$ and $E^R_{\rm tot}(t)$ is concurrent with the restructuring of the spectra from isotropic, KBK to strongly anisotropic distributions upon crossing n_β. Although at large times, $E^R_{\rm tot}$ is relatively small, the nonzonal modes play a crucial role in maintaining the zonal flows as they effectively preserve the upscale energy cascade.

Note that the evolution of the nonzonal spectrum $E_R(n)$ shown in Fig. 3b provides practically no information on a flow field transformation under the action of a β effect. Indeed, $E_R(n)$ retains an approximate KBK distribution, Eq. (13b), with nearly the same value of the coefficient C_K for both $n_\beta < n_m$ and $n_\beta > n_m$. Only the zonal spectrum, $E_Z(n)$, reflects the anisotropization by attaining a steeper slope.

For unsteady flows, the linear growth of the total energy, $E_{\rm tot} = \epsilon t$, yields the following expression for the Rhines scale:

$$n_R^{-1}(t) = \left(\frac{2U}{\beta}\right)^{1/2} \simeq \left(\frac{8\epsilon t}{\beta^2}\right)^{1/4}, \qquad (15)$$

which shows that n_R is time-dependent, $n_R \propto t^{-1/4}$. If the evolution of the moving energy front, $n_m(t)$, is plotted against $n_R(t)$, then one expects to detect two different power laws for the dependence of n_m on n_R. At the early stages, while $n_m(t) > n_\beta$ and the effect of the β term is not yet felt, n_m would evolve according to the $-3/2$ law, Eq. (8). Upon reaching n_β, as follows from Eqs. (7) and (15), n_m and n_R become proportional to each other. As estimated from the data, the numerical coefficient between n_m and n_R is approximately equal to 1.7. The $-3/2$ and $-1/4$ evolution laws and the transition between them are confirmed in Fig. 4 for the four experiments summarized in Table 1. The initial evolution is indeed according to the $-3/2$ law, which changes to the $-1/4$ law when n_m approaches n_β. Clearly, the change in the exponent of the evolution law is consistent with the change in the spectral slope shown in Fig. 3a. The transition between the two regimes is a complicated and nonuniversal process further exacerbated by the discrete character of the front propagation. Furthermore, the location of n_m in the transition area may be somewhat ambiguous as evident from Fig. 3a. Nevertheless, the transition wavenumbers are quite close to the values of n_β in Table 1 for all four runs. Figure 4 clearly demonstrates the absence of inverse cascade termination. Although a β effect is strong in the range $n_m < n_\beta$, the moving energy front, n_m, always reaches the lowest wavenumbers available in the system.

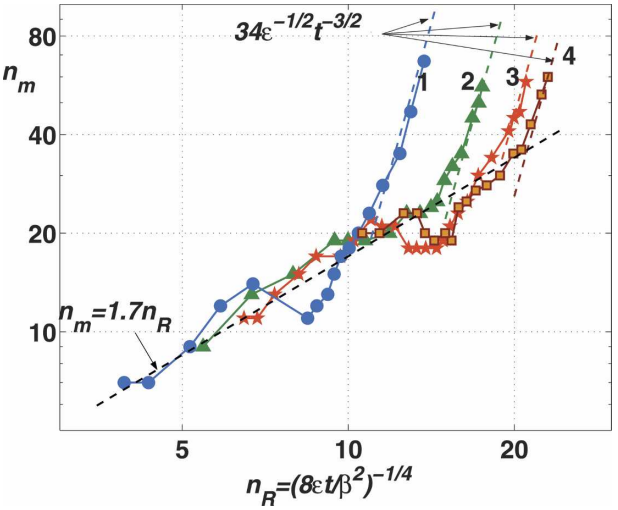

FIG. 4. The moving energy front, n_m, in unsteady simulations. The transition from the $-3/2$ to the $-1/4$ evolution law in the vicinity of the transitional wavenumbers n_β located at the intersections of the respective dashed lines is clearly visible for all four simulations. The figure demonstrates the absence of the halting wavenumber for the inverse energy cascade; the energy front can penetrate to the smallest wavenumbers available in the system.

Consider now a steady-state flow with a linear large-scale drag. By its very nature, such a flow is free of moving fronts; the march of the moving energy front had been damped by the drag. The final, stationary destination of the moving front, n_m, will now be identified with the friction wavenumber $n_{\rm fr}$ whose magnitude depends on the drag coefficient, λ, and, possibly, also on β and ϵ such that generally, one can write $n_{\rm fr} = f(\lambda, \beta, \epsilon)$. According to the Buckingham's Π theorem, this system is fully characterized by two functionally related nondimensional parameters, for instance,

$$\frac{n_{\rm fr}}{n_R} = f\left(\frac{n_\beta}{n_R}\right). \qquad (16)$$

The functional dependency varies according to a flow regime. Using an extensive series of long-term steady-state simulations of 2D turbulence with a β effect, we have derived a detailed classification of possible regimes in the space of parameters n_β and n_R (Galperin et al. 2006). These regimes are delineated by the dashed lines in Fig. 5. Two of these regimes, zonostrophic and

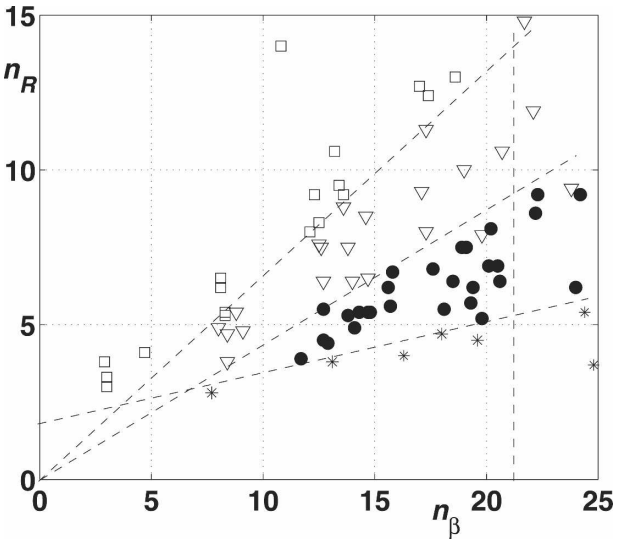

FIG. 5. Possible flow regimes in 2D turbulence with a β effect in the space of parameters n_R and n_β. The subspace of the friction-dominated regimes (unfilled squares) occupies the area to the left of the upper dashed line while the subspace of the zonostrophic regime (filled dots) outlined by the chain inequality (17) is confined to the area between the middle, bottom, and vertical dashed lines for the R133 experiments. For higher resolution, the vertical line moves to larger values of n_β.

friction-dominated, are of particular interest to the present study. The former is confined to the subspace outlined by the chain inequality

$$n_\xi \gtrsim 4n_\beta \gtrsim 8n_R \gtrsim 30. \tag{17}$$

This inequality instructs us that 1) the forcing acts on scales only weakly impacted by a β effect; 2) there exists a meaningful zonostrophic inertial range whose width is defined by the ratio n_β/n_R, and 3) there exists a sufficient number of the lowest modes to resolve the large-scale friction processes and avoid the large-scale condensation.

The friction-dominated or, briefly, friction regime occupies the subspace to the left of the top dashed line in Fig. 5 and is delineated by the inequality

$$\frac{n_\beta}{n_R} \lesssim 1.5. \tag{18}$$

In the friction regime, the zonostrophic inertial range is practically nonexistent; only the classical KBK inertial range may survive for $n > n_{\rm fr}$.

Let us consider now how Eq. (16) changes in different regimes. In the zonostrophic regime, when $n_\beta/n_R \gg 1$, the dependence on this parameter ceases (practically, this dependence becomes weak already at $n_\beta/n_R \gtrsim 2$) and one obtains $n_{\rm fr}/n_R \simeq$ constant. Let us calculate the numerical value of the proportionality constant. Since ϵ denotes the net part of the energy input that goes to the inverse cascade, the spectrally integrated energy balance equation reads

$$E_{\rm tot} = \frac{\epsilon}{2\lambda}. \tag{19}$$

Using this relationship, we obtain the Rhines wavenumber in the form

$$n_R = \left(\frac{\lambda\beta^2}{4\epsilon}\right)^{1/4}. \tag{20}$$

On the other hand, since the energy spectrum is comprised of a plateau for $n < n_{\rm fr}$ and the inertial part well approximated by Eq. (13a) for $n > n_{\rm fr}$, the total kinetic energy can be calculated by integrating this composite spectrum with respect to n. The integration yields an approximate relationship, $E_{\rm tot} \simeq (5/4)C_Z(\Omega/R)^2 n_{\rm fr}^{-4}$ (Galperin et al. 2001). Using this expression and Eq. (20), one can relate $n_{\rm fr}$ to n_R,

$$n_{\rm fr} = (10C_Z)^{1/4}\left(\frac{\lambda\beta^2}{4\epsilon}\right)^{1/4} \simeq 1.5n_R. \tag{21}$$

The coefficient 5/4 in the expression for $E_{\rm tot}$ above was stipulated by the assumption that the energy spectrum at $n < n_{\rm fr}$ is flat. This assumption is only an approximation; in real flows, this coefficient may need to be adjusted.

Equation (21) was verified in a series of simulations of the zonostrophic (filled dots in Fig. 5) and marginally zonostrophic (unfilled triangles adjacent to the zonostrophic region) regimes with widely varying values of λ ($5 \times 10^{-4} \le \lambda \le 2.5 \times 10^{-3}$), ϵ ($3.3 \times 10^{-9} \le \epsilon \le 9 \times 10^{-8}$), and Ω ($0.3 \le \Omega \le 2$). Note that due to the steep zonal spectrum, zonostrophic flows have low variability and require long-term integrations to assemble records sufficient for statistical analysis. Galperin and Sukoriansky (2005) have estimated that a record length of up to 100τ after attaining the steady state, $\tau = (2\lambda)^{-1}$ being the time scale associated with the large-scale drag, would be adequate for the spectral analysis. Accordingly, our steady-state simulations were of duration of about 60 to 100τ. The results of these simulations are summarized in Fig. 6. Note that the value of the coefficient in the correlation between $n_{\rm fr}$ and n_R in Eq. (21) had to be adjusted to 1.2. As one can see, the linear relationship between n_R and $n_{\rm fr}$ holds faithfully. One concludes, therefore, that, first, similarly to the unsteady case, a β effect does not halt the inverse energy cascade which is now damped by friction, and, second, in the zonostrophic regime, the Rhines scale is, in fact, a scale that characterizes the effect of the large-scale drag.

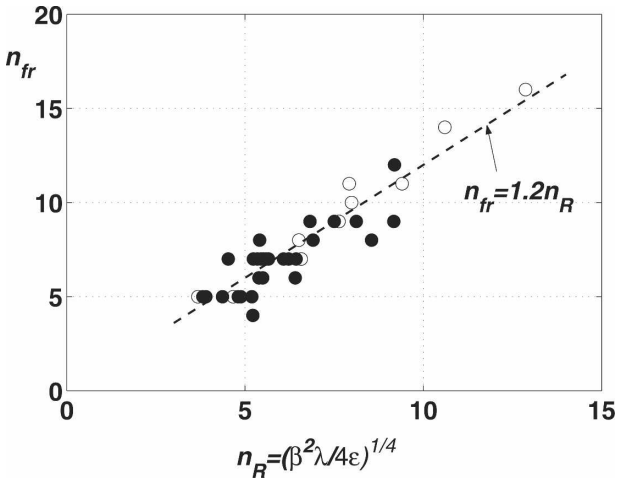

FIG. 6. The friction scale, $n_{\rm fr}$, determined as the intersection of the plateau and the -5 ranges in the energy spectrum, vs the Rhines scale, n_R, in simulations of the zonostrophic (filled dots) and marginally zonostrophic (empty dots) regimes with a linear large-scale drag.

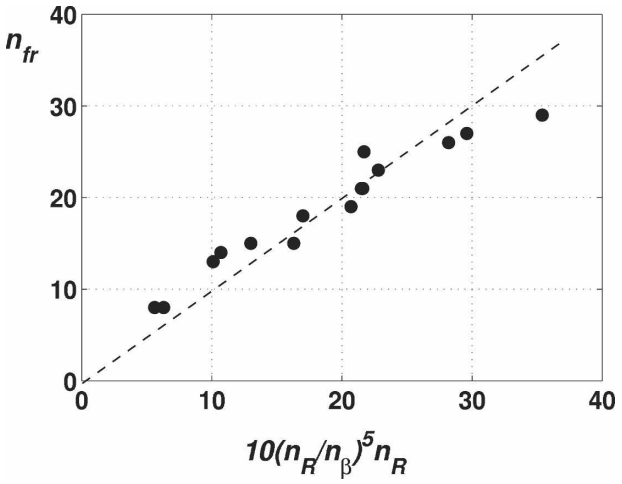

FIG. 7. The correlation between the actual and theoretical values of $n_{\rm fr}$ calculated using (23) in simulations of the large-scale drag dominated 2D turbulence with a β effect.

In the friction regime, the drag may be so strong that its impact extends to the scales where the flow is unaffected by β [this aspect was considered by Danilov and Gurarie (2002), Smith et al. (2002), James and Gray (1986)]. The functional relationship between $n_{\rm fr}/n_R$ and n_β/n_R can then be established using the assumption that the energy spectrum is isotropic and described by the KBK distribution, Eq. (3). The total kinetic energy in this case is given by the expression $E_{\rm tot} \simeq (3/2)C_K\epsilon^{2/3}n_{\rm fr}^{-2/3}$, where $n_{\rm fr}$ is the wavenumber with the maximum energy. Using the energy balance equation, Eq. (19), we obtain

$$n_{\rm fr} = (3C_K)^{3/2}(\lambda^3/\epsilon)^{1/2}. \tag{22}$$

Using Eq. (22) and the definitions of n_β, Eq. (14), and n_R, Eq. (20), we further find

$$n_{\rm fr} = (12C_Z)^{3/2}\left(\frac{n_{\rm R}}{n_\beta}\right)^5 n_R \simeq 14.7\left(\frac{n_R}{n_\beta}\right)^5 n_R. \tag{23}$$

This relationship is very different from the one derived for the zonostrophic regime, Eq. (21), because now $n_{\rm fr}$ depends on ϵ and is independent of β such that the proportionality between $n_{\rm fr}$ and n_R is lost. Summarizing, we note that the dependence of $n_{\rm fr}$ on n_R given by Eq. (16) has two asymptotic cases pertaining to the zonostrophic and friction regimes. In the former, $n_{\rm fr}$ and n_R are related linearly and are generally quite close while in the latter they diverge from each other by a stiff power law. In the intermediate cases, the relationship between $n_{\rm fr}$ on n_R can be expected to be nonlinear and complicated which explains why the scaling of the zonal jets' width with n_R^{-1} has been so evasive in diverse flows.

Equation (23) has been validated in numerical simulations with large values of the drag coefficient, λ, which was chosen such that $n_\beta/n_R \lesssim 1.5$. These simulations are shown as unfilled squares in Fig. 5. Figure 7 shows a good agreement between the actual values of $n_{\rm fr}$ and those calculated from Eq. (23) with the coefficient adjusted to 10.

There still remains a question about the proper scaling of the width of the zonal jets which in some studies was found to be close to n_R^{-1}. When the jets have approximately homogeneous spatial distribution, their width can be estimated from the number of the jets, $n_{\rm jet}$. It is of interest, therefore, to compare $n_{\rm jet}$ with $n_{\rm fr}$ and n_R.

Figure 8, derived from simulations of the zonostrophic regime, indicates that $n_{\rm jet} \simeq n_R$. The spread of the data points is caused by the discreteness of $n_{\rm jet}$. In the range $4 \le n_{\rm jet} \le 10$, for example, unavoidable unity deviations appear like a 10%–25% noise. In fact, given this uncertainty, n_R provides a faithful estimation of the number of the zonal jets. Using the correlation between $n_{\rm fr}$ and n_R shown in Fig. 6, one concludes that both $n_{\rm fr}^{-1}$ and n_R^{-1} are appropriate scaling parameters for the jets' width in the zonostrophic regime. We have also attempted to scale $n_{\rm jet}$ with n_R calculated using the nonzonal velocities only. In that case, the correlation between $n_{\rm jet}$ and n_R was considerably worse than that in Fig. 8 and, therefore, it is not shown here.

We now want to analyze the interplay between tur-

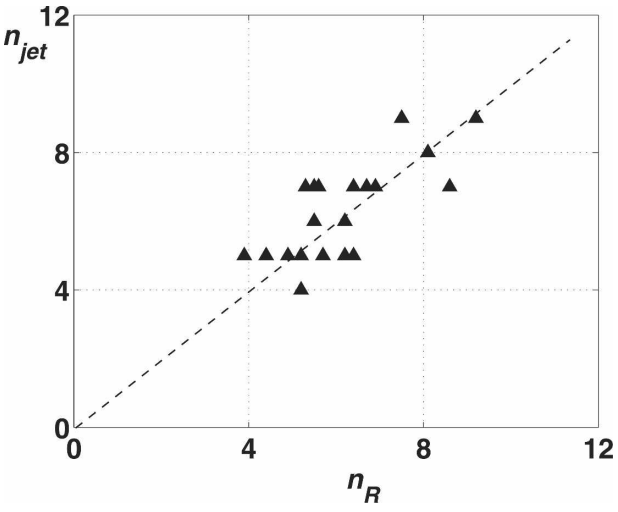

FIG. 8. The correlation between the number of the zonal jets, n_{jet}, estimated from the velocity profile in the physical space, and n_R obtained from numerical simulations of the zonostrophic regime.

bulence and Rossby waves in order to determine whether n_R (or n_β) separate turbulence and Rossby wave regions or turbulence and waves coexist in some range of scales. To answer this question, it is instructive to analyze the Fourier transform of the two-time velocity autocorrelation function given by

$$U(\omega, m, n) = \frac{n(n+1)}{4} \langle |\psi_n^m(\omega)|^2 \rangle, \tag{24}$$

where $\psi_n^m(\omega)$ is a time Fourier transformed spectral coefficient $\psi_n^m(t)$ defined in Eq. (10). In 2D turbulence without Rossby waves, $U(\omega, m, n)$ would be expected to have a symmetric bell shape around the zero frequency. When the waves are present, they cause $U(\omega, m, n)$ to develop spikes at frequencies corresponding to the dispersion relation. The correlation function $U(\omega, m, n)$ is therefore a convenient tool to establish and/or diagnose the dispersion relations in data. A similar approach based upon the analysis of the autocorrelation function of the sea surface elevation obtained from the satellite altimetry has been used by other researchers (see, e.g., Glazman and Cheng 1999; Glazman and Weichman 2005) to diagnose the baroclinic Rossby waves in the ocean. The results of our analysis are shown in Figs. 9 and 10 for the friction dominated and zonostrophic regimes, respectively. In the former case, for small wavenumbers, Rossby waves produce sharp spikes almost exactly corresponding to the linear dispersion relation (11). Similar spikes also appear at higher wavenumbers although they are not as sharp because they are progressively broadened by turbulence. As evident from Fig. 9, Rossby waves are present at n far exceeding both n_R and n_β indicating that there is no separation between Rossby waves and turbulence; both processes coexist in a wide range of scales. Figure 10 depicts a more complicated wave–turbulence interaction. As in Fig. 9, the spectral spikes at small n are sharp but now they begin to show signs of a strong wave–turbulence interaction. At larger n, due to a stronger turbulence, the spikes broaden and become displaced from the values stipulated by the linear dispersion relationship. This behavior is indicative of a complex nature of turbulence–wave interaction in the case of the zonostrophic regime, which may manifest itself in the development of the Rossby wave frequency shift or in the appearance of nonlinear waves different from Rossby waves. Similarly to Fig. 9, Rossby waves and turbulence coexist for wavenumbers exceeding both n_R and n_β. Note that the wave–turbulence interaction is stronger and more subtle in the zonostrophic than in the friction-dominated regime; a more detailed investigation of this interaction will be given elsewhere. An important result from this study is that there exists neither a sharp transition between linear and nonlinear regimes nor a distinct boundary between turbulence and Rossby wave spectral ranges. This result reinforces our earlier conclusion that neither n_β nor n_R can be associated with the turbulence–Rossby wave transition.

5. Discussion and conclusions

One of the main results of the presented here theoretical analysis and numerical simulations is the conclusion that a nondissipative extra strain in the vorticity equation, a β term, can cause no arrest of the inverse energy cascade in 2D turbulence. The effect of the β term on energy transfer manifests in cascade anisotropization and formation of quasi-1D structures, zonal jets. This result can be likened to that in 3D flows with pure rotation where nondissipative extra strains are brought about by the Coriolis force. Again, turbulent cascade in this case is not arrested but anisotropized leading to self-organization of the flow field into quasi-2D, large-scale columnar vortices aligned with the rotation axis (Smith and Lee 2005). Even in the case when extra strains do enter the kinetic energy equation as sink terms, they cannot totally suppress turbulent cascade. For example, in the case of 3D flows with stable stratification, there also exists strong anisotropization. Along the direction of the extra force (i.e., the gravity), turbulent exchange diminishes, but in the normal planes, turbulence is not suppressed and may even be enhanced (Sukoriansky et al. 2005; Smith and Waleffe

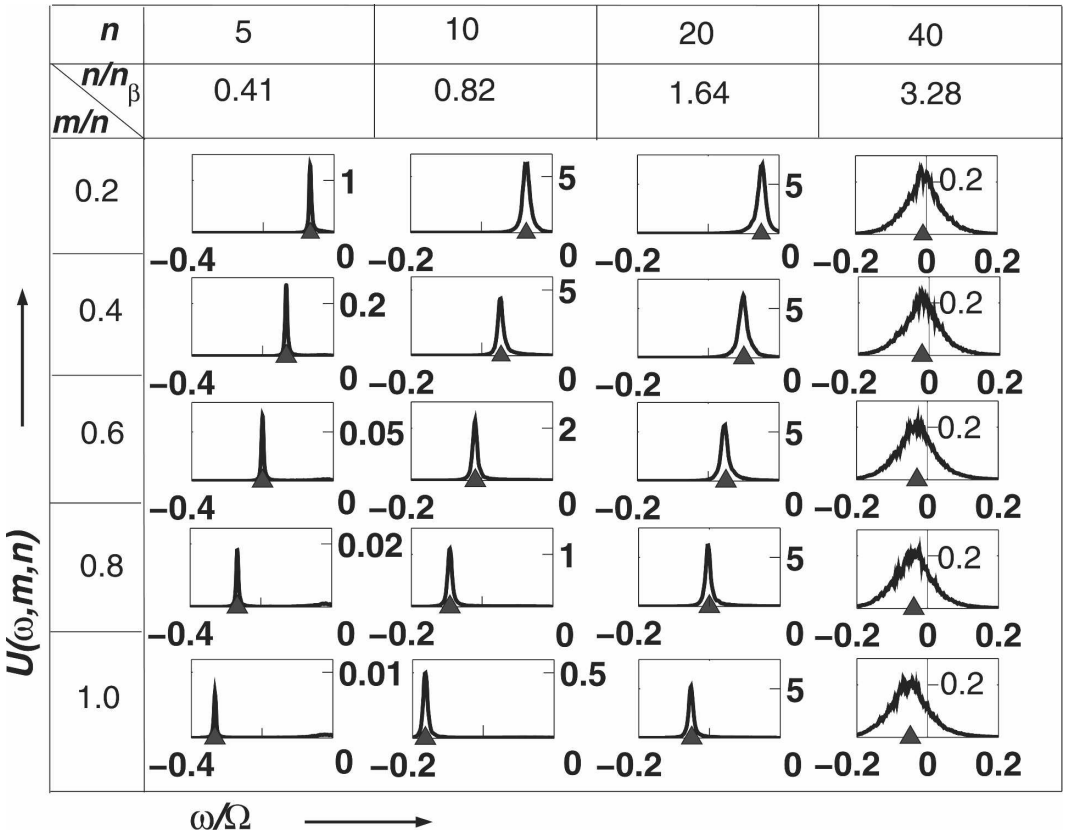

FIG. 9. The velocity autocorrelation function, $U(\omega, m, n) \times 10^7$, for the friction dominated regime; $n_R \simeq 9$, $n_\beta \simeq 12$. The triangles correspond to the linear dispersion relation (11).

2002). In all these cases, the extra strains support various types of linear waves, which can coexist with turbulence in wide ranges of scales.

Our simulations revealed neither a sharp separation between the regions of turbulence and wave domination nor a large-scale threshold of the Rossby wave propagation. The opposite is true; similarly to the internal and inertial waves, Rossby waves can coexist with turbulence in a wide range of scales. Rather than being a scale of the cascade arrest, the Rhines scale may characterize many different phenomena. In the present study, this conclusion is illustrated by two examples. In unsteady flows, L_R appears as a scale of the largest energy containing structures, while in a steady-state zonostrophic regime, the Rhines scale coincides with the scale of the large-scale friction. Furthermore, it is shown that the relationship between the Rhines and friction scales is not universal and depends on the flow regime. It is not surprising, therefore, that L_R has been used as a scaling parameter characterizing various aspects of flows with a β effect. As an example, one may recall that the scaling with L_R has been applied both to the equatorial (Hide 1966) and off-equatorial (Williams 1978) Jovian jets although their widths are quite different. Generally, the Rhines scale is a basic dimensional parameter in flows not necessarily related to geostrophic turbulence where a β effect is a salient feature (see, e.g., Pedlosky 1998; Nof et al. 2004).

As was shown in section 4, a nondimensional parameter $R_\beta = n_\beta/n_R$ plays a key role in quasi-2D, steady-state turbulent flows with a β effect. By virtue of determining the type of a flow regime, this parameter reveals important information on various aspects of large-scale circulations. Recasting R_β in terms of the basic flow parameters, we obtain

$$R_\beta = 2^{1/2}\left(\frac{C_Z}{C_K}\right)^{3/10}\left(\frac{\beta U^5}{\epsilon^2}\right)^{1/10} \simeq 0.7\left(\frac{\beta U^5}{\epsilon^2}\right)^{1/10}. \tag{25}$$

This number can also be defined in terms of the external flow parameters, λ, β, and ϵ,

$$R_\beta = 2^{1/2}\left(\frac{C_Z}{C_K}\right)^{3/10}\left(\frac{\beta^2\epsilon}{\lambda^5}\right)^{1/20} \simeq 0.7\left(\frac{\beta^2\epsilon}{\lambda^5}\right)^{1/20}. \tag{26}$$

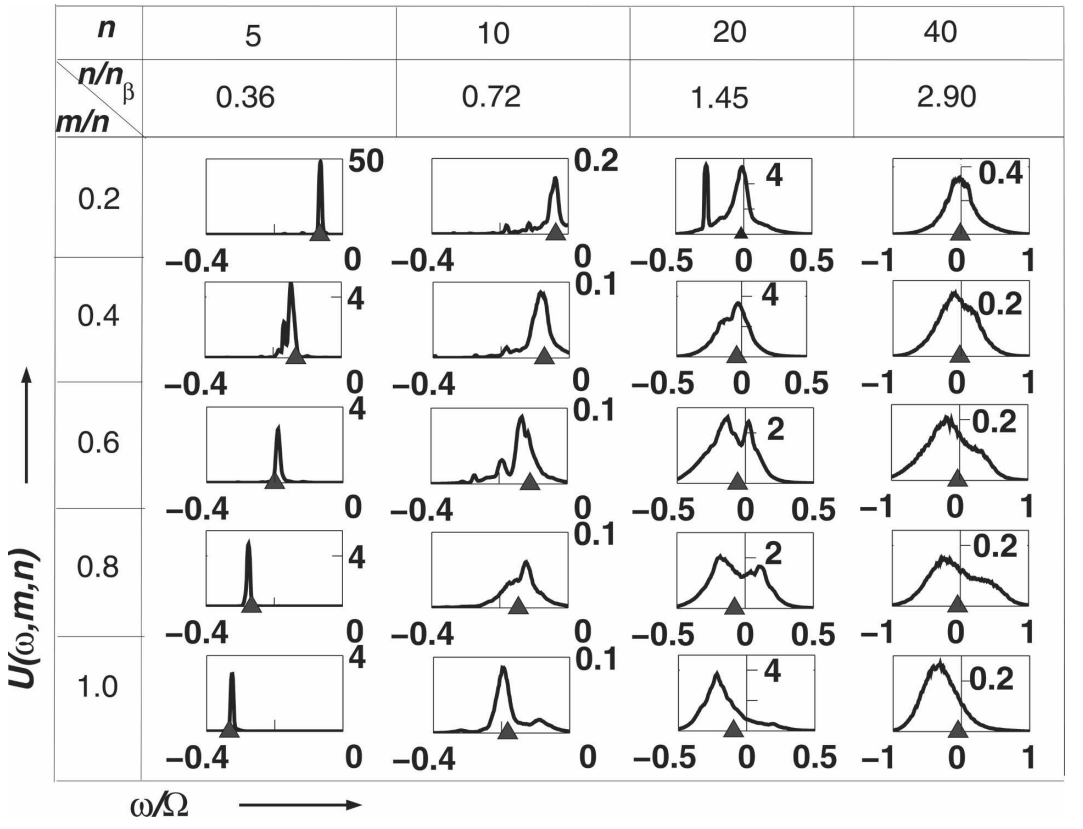

FIG. 10. The velocity autocorrelation function, $U(\omega, m, n)$, for the zonostrophic regime; $n_R \simeq 5$, $n_\beta \simeq 14$. The scaling coefficients for U are 10^5 for $n = 5$ and 10 and 10^8 for $n = 20$ and 40. The triangles correspond to the linear dispersion relation (11).

The zonostrophic regime is characterized by $R_\beta > 2$ (in addition to the smallness of the Burger number, Bu; see e.g., Galperin et al. 2006) while for the friction-dominated regime, $R_\beta \lesssim 1.5$. The range $1.5 \lesssim R_\beta \lesssim 2$ corresponds to a transitional regime whose properties are not universal. It is instructive to calculate the values of R_β for different environments. To illustrate the significance of R_β, we shall consider a wide variety of environments with small Bu ranging from the small-scale turntable used in the Grenoble experiment (Read et al. 2004, 2007) to the terrestrial oceans and to the solar giant planets' weather layers.

For the Grenoble experiment, using the parameters reported in Read et al. (2007), one obtains $R_\beta \in (0.5, 2.3)$; that is, the experimental flow was marginally zonostrophic. It is not surprising, therefore, that the flow field obtained in some experiments exhibited zonation, spectral anisotropization, and build up of the zonal spectrum described by Eq. (13a).

For the oceanic flows, the magnitude of ϵ can be estimated between 10^{-9} and 10^{-11} $m^2\,s^{-3}$, the latter value follows, for example, from the realistic, eddy-resolving simulations by Nakano and Hasumi (2005). With such values of ϵ and U of the order of 10 cm s^{-1}, one finds that $R_\beta \in (1, 2.8)$. Similarly to the Grenoble experiment, the oceanic flows are on the verge between the zonostrophic and friction-dominated regimes. Visually, oceanic flows are quite erratic as would be expected in the transitional regime. However, averaging in time reveals zonation (see, e.g., Maximenko et al. 2005; Ollitrault et al. 2006) and spectral anisotropization (Zang and Wunsch 2001) suggesting that R_β is rather close to 2. In addition, some numerical models show the build up of the zonal spectrum according to Eq. (13a) (Galperin et al. 2004). Even though the zonostrophic inertial range in the ocean is small and the barotropic currents are relatively weak, by virtue of the zonation that penetrates through considerable depth these currents can still play an important role in the dynamic and transport processes. Studies of these processes are now becoming an area of an active research (see, e.g., Galperin et al. 2004; Smith 2005; Richards et al. 2006; Ollitrault et al. 2006; Nadiga 2006; Eden 2006).

For the solar giant planets, ϵ can be estimated at 10^{-8} $m^2\,s^{-3}$ (Galperin et al. 2006) yielding $R_\beta \sim 10$, 25, 30, and 40 for Jupiter, Saturn, Uranus, and Neptune, re-

spectively. The large values of R_β on all four solar giant planets indicate that their atmospheric circulations feature well established zonostrophic regimes. Indeed, the energy spectra of the zonal flows on these planets are consistent with Eq. (13a) in both the slope and the magnitude (Galperin et al. 2001; Sukoriansky et al. 2002).

The present results emphasize the importance of the barotropic mode in flows with a small Burger number. In the case of the zonostrophic regime with a profound inertial range (or large R_β), the barotropic mode contains most of the kinetic energy and hence governs the large-scale circulation and its energetics. As shown in Sukoriansky et al. (2002), the total kinetic energy of a circulation in this regime is determined by Ω, R, and n_{fr} only and is independent of the external forcing or the potential energy conversion rate unless these dependencies are implicitly embedded in the friction wavenumber n_{fr} the physical mechanism of which is not always well understood and is a subject of an ongoing research (see, e.g., Müller et al. 2005).

Acknowledgments. We are grateful to Drs P. L. Read, M. E. McIntyre, W. R. Young, A. Showman, H.-P. Huang, and N. Maximenko for numerous discussions and comments during the course of this research. Thoughtful comments from anonymous reviewers helped us to improve and clarify the manuscript. Partial support of this study by the ARO Grant W911NF-05-1-0055 and the Israel Science Foundation Grant 134/03 is greatly appreciated.

REFERENCES

Balk, A., 1991: A new invariant for Rossby wave systems. *Phys. Lett. A,* **155,** 20–24.

——, 2005: Angular distribution of Rossby wave energy. *Phys. Lett. A,* **345,** 154–160.

——, and F. van Heerden, 2006: Conservation style of the extra invariant for Rossby waves. *Physica D,* **223,** 109–120.

Barry, L., G. Craig, and J. Thuburn, 2002: Poleward heat transport by the atmospheric heat engine. *Nature,* **415,** 774–777.

Boer, G., 1983: Homogeneous and isotropic turbulence on the sphere. *J. Atmos. Sci.,* **40,** 154–163.

——, and T. Shepherd, 1983: Large-scale two-dimensional turbulence in the atmosphere. *J. Atmos. Sci.,* **40,** 164–184.

Bradshaw, P., 1973: Effects of streamline curvature on turbulent flow. AGARDograph Rep. 169, Advisory Group for Aerospace Research and Development, Paris, France, 128 pp.

Carnevale, G., and P. Martin, 1982: Field theoretical techniques in statistical fluid dynamics: With application to nonlinear wave dynamics. *Geophys. Astrophys. Fluid Dyn.,* **20,** 131–164.

Chekhlov, A., S. Orszag, S. Sukoriansky, B. Galperin, and I. Staroselsky, 1996: The effect of small-scale forcing on large-scale structures in two-dimensional flows. *Physica D,* **98,** 321–334.

Cho, J.-K., and L. Polvani, 1996: The emergence of jets and vortices in freely evolving, shallow-water turbulence on a sphere. *Phys. Fluids,* **8,** 1531–1552.

Danilov, S., and D. Gurarie, 2002: Rhines scale and spectra of the β-plane turbulence with bottom drag. *Phys. Rev. E,* **65,** doi:10.1103/PhysRevE.65.067301.

Eden, C., 2006: Middepth equatorial tracer tongues in a model of the Atlantic Ocean. *J. Geophys. Res.,* **111,** C12025, doi:10.1029/2006JC003565.

Galperin, B., and S. Sukoriansky, 2005: Energy spectra and zonal flows on the β plane, on a rotating sphere, and on giant planets. *Marine Turbulence: Theories, Observations, and Models,* H. Baumert, J. Simpson, and J. Sündermann, Eds., Cambridge University Press, 472–493.

——, ——, and H.-P. Huang, 2001: Universal n^{-5} spectrum of zonal flows on giant planets. *Phys. Fluids,* **13,** 1545–1548.

——, H. Nakano, H.-P. Huang, and S. Sukoriansky, 2004: The ubiquitous zonal jets in the atmospheres of giant planets and Earth's oceans. *Geophys. Res. Lett.,* **31,** L13303, doi:10.1029/2004GL019691.

——, S. Sukoriansky, N. Dikovskaya, P. Read, Y. Yamazaki, and R. Wordsworth, 2006: Anisotropic turbulence and zonal jets in rotating flows with a β-effect. *Nonlinear Proc. Geophys.,* **13,** 83–98.

Glazman, R., and B. Cheng, 1999: Altimeter observations of baroclinic oceanic inertia-gravity wave turbulence. *Proc. Roy. Soc. London,* **455,** 91–123.

——, and P. Weichman, 2005: Meridional component of oceanic Rossby wave propagation. *Dyn. Atmos. Oceans,* **38,** 173–193.

Held, I., 1999: The macroturbulence of the troposphere. *Tellus,* **51A,** 59–70.

——, and V. Larichev, 1996: A scaling theory for horizontally homogeneous, baroclinically unstable flow on a beta plane. *J. Atmos. Sci.,* **53,** 946–952.

Hide, R., 1966: On the circulation of the atmospheres of Jupiter and Saturn. *Planet. Space Sci.,* **14,** 669–675.

Holloway, G., 1986: Considerations on the theory of temperature spectra in stably stratified turbulence. *J. Phys. Oceanogr.,* **16,** 2179–2183.

——, and M. Hendershott, 1977: Stochastic closure for nonlinear Rossby waves. *J. Fluid Mech.,* **82,** 747–765.

Huang, H.-P., and W. Robinson, 1998: Two-dimensional turbulence and persistent zonal jets in a global barotropic model. *J. Atmos. Sci.,* **55,** 611–632.

——, B. Galperin, and S. Sukoriansky, 2001: Anisotropic spectra in two-dimensional turbulence on the surface of a rotating sphere. *Phys. Fluids,* **13,** 225–240.

James, I., 1987: Suppression of baroclinic instability in horizontally sheared flows. *J. Atmos. Sci.,* **44,** 3710–3720.

——, and L. Gray, 1986: Concerning the effect of surface drag on the circulation of a baroclinic planetary atmosphere. *Quart. J. Roy. Meteor. Soc.,* **112,** 1231–1250.

LaCasce, J., and J. Pedlosky, 2004: The instability of Rossby basin modes and the oceanic eddy field. *J. Phys. Oceanogr.,* **34,** 2027–2041.

Lapeyre, G., and I. Held, 2003: Diffusivity, kinetic energy dissipation, and closure theories for the poleward eddy heat flux. *J. Atmos. Sci.,* **60,** 2907–2916.

Lilly, D. K., 1972: Numerical simulation study of two-dimensional turbulence. *Geophys. Fluid Dyn.,* **3,** 289–319.

Majda, A., and X. Wang, 2006: *Nonlinear Dynamics and Statistical Theories for Basic Geophysical Flows.* Cambridge University Press, 551 pp.

Maximenko, N., B. Bang, and H. Sasaki, 2005: Observational evi-

dence of alternating zonal jets in the world ocean. *Geophys. Res. Lett.,* **32,** L12607, doi:10.1029/2005GL022728.

McIntyre, M., 2001: Balance, potential-vorticity inversion, lighthill radiation, and the slow quasimanifold. *IUTAM Symposium on Advances in Mathematical Modeling of Atmosphere and Ocean Dynamics,* P. Hodnett, Ed., Kluwer Academic, 45–68.

McWilliams, J., 2006: *Fundamentals of Geophysical Fluid Dynamics.* Cambridge University Press, 249 pp.

Miesch, M., 2003: Numerical modeling of the solar tachocline. II. Forced turbulence with imposed shear. *Astrophys. J.,* **586,** 663–684.

Müller, P., J. McWilliams, and M. Molemaker, 2005: Routes to dissipation in the ocean: The two-dimensional/three-dimensional turbulence conundrum. *Marine Turbulence: Theories, Observations, and Models,* H. Baumert, J. Simpson, and J. Sündermann, Eds., Cambridge University Press, 397–405.

Nadiga, B., 2006: On zonal jets in oceans. *Geophys. Res. Lett.,* **33,** L10601, doi:10.1029/2006GL025865.

Nakano, H., and H. Hasumi, 2005: A series of zonal jets embedded in the broad zonal flows in the Pacific obtained in eddy-permitting ocean general circulation models. *J. Phys. Oceanogr.,* **35,** 474–488.

Nof, D., S. Van Gorder, and T. Pichevin, 2004: A different outflow length scale? *J. Phys. Oceanogr.,* **34,** 793–804.

Nozawa, T., and S. Yoden, 1997: Formation of zonal band structure in forced two-dimensional turbulence on a rotating sphere. *Phys. Fluids,* **9,** 2081–2093.

Ollitrault, M., M. Lankhorst, D. Fratantoni, P. Richardson, and W. Zenk, 2006: Zonal intermediate currents in the equatorial Atlantic Ocean. *Geophys. Res. Lett.,* **33,** L05605, doi:10.1029/2005GL025368.

Panetta, R., 1993: Zonal jets in wide baroclinically unstable regions: Persistence and scale selection. *J. Atmos. Sci.,* **50,** 2073–2106.

Pedlosky, J., 1998: *Ocean Circulation Theory.* 2d ed. Springer, 453 pp.

Read, P., 2005: From mixing to geostrophy: Geostrophic turbulence in atmospheres, oceans, and the laboratory. *Marine Turbulence: Theories, Observations, and Models,* H. Baumert, J. Simpson, and J. Sündermann, Eds., Cambridge University Press, 406–422.

——, Y. Yamazaki, S. Lewis, P. Williams, K. Miki-Yamazaki, J. Sommeria, H. Didelle, and A. Fincham, 2004: Jupiter's and Saturn's convectively driven banded jets in the laboratory. *Geophys. Res. Lett.,* **31,** L22701, doi:10.1029/2004GL020106.

——, ——, ——, ——, R. Wordsworth, K. Miki-Yamazaki, J. Sommeria, and H. Didelle, 2007: Dynamics of convectively driven banded jets in the laboratory. *J. Atmos. Sci.,* in press.

Rhines, P., 1975: Waves and turbulence on a beta-plane. *J. Fluid Mech.,* **69,** 417–443.

——, 1979: Geostrophic turbulence. *Annu. Rev. Fluid Mech.,* **11,** 401–411.

Richards, K., N. Maximenko, F. Bryan, and H. Sasaki, 2006: Zonal jets in the Pacific Ocean. *Geophys. Res. Lett.,* **33,** L03605, doi:10.1029/2005GL024645.

Rose, H., and P. Sulem, 1978: Fully developed turbulence and statistical mechanics. *J. Phys.,* **39,** 441–484.

Schneider, T., 2004: The tropopause and the thermal stratification in the extratropics of a dry atmosphere. *J. Atmos. Sci.,* **61,** 1317–1340.

——, 2006: The general circulation of the atmosphere. *Annu. Rev. Earth Planet. Sci.,* **34,** 655–688.

Smith, K., 2005: Tracer transport along and across coherent jets in two-dimensional turbulent flow. *J. Fluid Mech.,* **544,** 133–142.

——, G. Boccaletti, C. Henning, I. Marinov, C. Tam, I. Held, and G. Vallis, 2002: Turbulent diffusion in the geostrophic inverse cascade. *J. Fluid Mech.,* **469,** 13–48.

Smith, L., and V. Yakhot, 1993: Bose condensation and small-scale structure generation in a random force driven 2D turbulence. *Phys. Rev. Lett.,* **71,** 352–355.

——, and ——, 1994: Finite-size effects in forced two-dimensional turbulence. *J. Fluid Mech.,* **274,** 115–138.

——, and F. Waleffe, 1999: Transfer of energy to two-dimensional large scales in forced, rotating three-dimensional turbulence. *Phys. Fluids,* **11,** 1608–1622.

——, and ——, 2002: Generation of slow large scales in forced rotating stratified turbulence. *J. Fluid Mech.,* **451,** 145–168.

——, and Y. Lee, 2005: On near resonances and symmetry breaking in forced rotating flows at moderate Rossby number. *J. Fluid Mech.,* **535,** 111–142.

Sukoriansky, S., B. Galperin, and A. Chekhlov, 1999: Large scale drag representation in simulations of two-dimensional turbulence. *Phys. Fluids,* **11,** 3043–3053.

——, ——, and N. Dikovskaya, 2002: Universal spectrum of two-dimensional turbulence on a rotating sphere and some basic features of atmospheric circulation on giant planets. *Phys. Rev. Lett.,* **89,** doi:10.1103/PhysRevLett.89.124501.

——, ——, and I. Staroselsky, 2005: A quasinormal scale elimination model of turbulent flows with stable stratification. *Phys. Fluids,* **17,** doi:10.1063/1.2009010.

Vallis, G., 2006: *Atmospheric and Oceanic Fluid Dynamics.* Cambridge University Press, 745 pp.

——, and M. Maltrud, 1993: Generation of mean flows and jets on a beta plane and over topography. *J. Phys. Oceanogr.,* **23,** 1346–1362.

Vasavada, A., and A. Showman, 2005: Jovian atmospheric dynamics: An update after Galileo and Cassini. *Rep. Prog. Phys.,* **68,** 1935–1996.

Williams, G., 1975: Jupiter's atmospheric circulation. *Nature,* **257,** 778.

——, 1978: Planetary circulations. Part I: Barotropic representation of Jovian and terrestrial turbulence. *J. Atmos. Sci.,* **35,** 1399–1426.

Zang, X., and C. Wunsch, 2001: Spectral description of low-frequency oceanic variability. *J. Phys. Oceanogr.,* **31,** 3073–3095.